Atmospheric and Oceanic Science Letters 16 (2023) 100320

Contents lists available at ScienceDirect

Atmospheric and Oceanic Science Letters

journal homepage:
http://www.keaipublishing.com/en/journals/atmospheric-and-oceanic-science-letters/

Strength of the North African monsoon in the Last Interglacial and under future warming

Jiazhi He[a], Weiyi Sun[a,*], Jing Wang[a], Bin Wang[b], Jian Liu[a,c,d]

[a] Key Laboratory for Virtual Geographic Environment, Ministry of Education, State Key Laboratory Cultivation Base of Geographical Environment Evolution of Jiangsu Province, Jiangsu Center for Collaborative Innovation in Geographical Information Resource Development and Application, School of Geography Science, Nanjing Normal University, Nanjing, China
[b] Department of Atmospheric Sciences and Atmosphere–Ocean Research Center, University of Hawaii at Manoa, Honolulu, HI, USA
[c] Jiangsu Provincial Key Laboratory for Numerical Simulation of Large Scale Complex Systems, School of Mathematical Science, Nanjing Normal University, Nanjing, China
[d] Open Studio for the Simulation of Ocean-Climate-Isotope, Qingdao National Laboratory for Marine Science and Technology, Qingdao, China

ARTICLE INFO

Keywords:
North african monsoon
Precipitation variability
Last interglacial
Global warming
关键词:
北非季风
降水变率
末次间冰期
全球变暖

ABSTRACT

The authors explore the response of the Northern African (NAF) monsoon to orbital forcing in the Last Interglacial (LIG) compared with its response to greenhouses gas (GHG) forcing under the SSP5-8.5 scenario simulated in CMIP6. When the summer surface air temperature increases by 1 °C over the Northern Hemisphere, the NAF monsoon precipitation and its variability during the LIG increase by approximately 51% and 22%, respectively, which is much greater than under SSP5-8.5 (2.8% and 4.3%, respectively). GHG forcing enhances the NAF monsoon mainly by increasing the atmospheric moisture, while the LIG's orbital forcing intensifies the NAF monsoon by changing the monsoon circulation. During the LIG, models and data reconstructions indicate a salient hemispheric thermal contrast between the North and South Atlantic, strengthening the mean-state NAF monsoon precipitation. The interhemispheric temperature contrast enhances atmosphere–ocean interaction and the covariability of the northward sea surface temperature gradient and Saharan low, strengthening the NAF monsoon variability.

摘要

与人为强迫引起的全球变暖相比, 末次间冰期是轨道强迫引起的过去80万年来最暖的一个间冰期, 但鲜有人研究末次间冰期中北非季风的响应. 因此, 本文基于CMIP6多模式模拟结果对比研究了末次间冰期和SSP5–8.5情景下北非季风的响应, 发现末次间冰期下北非季风平均降水及其降水变率均远大于SSP5–8.5情景下的结果. 轨道强迫导致的北大西洋暖于南大西洋增加了北非季风环流和平均降水, 同时, 南北大西洋海温梯度变化通过增强热带北大西洋的海气相互作用增大了海温梯度和撒哈拉低压的变率, 从而增强了北非季风降水变率.

1. Introduction

The Last Interglacial (LIG; 129–116 ka), a past warm epoch, provides a different perspective on understanding the mechanism of future climate change. There is an equilibrium simulation for the LIG, named *lig127k*, included in phase 6 of the Coupled Model Intercomparison Project (CMIP6) and in phase 4 of the Paleoclimate Modeling Intercomparison Project (PMIP4) (O'Neill et al., 2016; Otto-Bliesner et al., 2017). The *lig127k* experiment is designed to understand the climate response to strong orbital forcing, while the atmospheric greenhouse gas (GHG) concentration is similar to the pre-industrial (PI) condition (Otto-Bliesner et al., 2017). The LIG orbital forcing results in a stronger boreal summer insolation in the Northern Hemisphere (NH) than the Southern Hemisphere (SH) relative to the PI, which enhances the interhemispheric thermal contrast. Compared to the LIG experiment, the SSP5-8.5 experiment, an extreme GHG emission scenario, represents a high future pathway toward a radiative forcing of 8.5 W m^{-2} in 2100. Since previous studies indicate that the Northern African (NAF) monsoon is quite sensitive to climate change (e.g., Wang et al., 2021; Cao et al., 2020, 2022), it is important to compare the response of the NAF monsoon under the LIG with the SSP5-8.5 scenario.

In terms of the mechanism of the mean-state NAF monsoon change, previous studies have found that the increased NAF monsoon precipitation under the SSP2–4.5 scenario is correlated with the warming in the North Atlantic and Sahara region, which enhances the land–sea thermal contrast and meridional temperature gradient over the Atlantic Ocean (e.g., Jin et al., 2020). Using the moisture budget analysis, D'Agostino et al. (2019) found that the increased atmospheric moisture term also contributes to the enhancement of NAF monsoon rainfall under the RCP8.5 scenario. However, during the LIG, it is

* Corresponding author.
E-mail address: weiyisun@njnu.edu.cn (W. Sun).

https://doi.org/10.1016/j.aosl.2022.100320
Received 10 October 2022; Revised 16 November 2022; Accepted 1 December 2022
Available online 6 December 2022

not known whether the enhanced mean-state NAF monsoon is mainly caused by the increased water vapor or the increased circulation effect induced by the land–sea thermal contrast or the meridional temperature gradient.

Regarding the mechanism of the NAF monsoon variability, previous studies have found that the variability of tropical Atlantic sea surface temperature (SST) is the primary driver for the NAF monsoon variability on the interannual time scale (e.g., Giannini et al., 2003). Climate models suggest an increase in the interannual variability of NAF monsoon precipitation under greenhouse warming, which is induced by increased atmospheric moisture feedback (Hsu et al., 2013; Ni and Hsu, 2018; Pendergrass et al., 2017; Zhang et al., 2021). Meanwhile, many studies have found that the positive or negative phase of the Atlantic Multidecadal Oscillation (AMO) contributes to the decadal variability of the NAF monsoon (Dai, 2011; Diakhaté et al., 2019; Folland et al., 1986; Giannini et al., 2003; Hoerling et al., 2006; Knight et al., 2006; Mohino et al., 2011; Trenberth et al., 2000). For example, the positive phase of the AMO can reinforce the westerly winds into the Sahel by strengthening the Saharan heat low, and enhance the low-level West African westerly jet (Martin and Thorncroft, 2014; Pu and Cook, 2010). However, it is unknown whether the above mechanisms that affect the NAF monsoon variability are equally applicable in the LIG.

Some proxy data show that the West African monsoon rainfall increases significantly during the LIG (Weldeab et al., 2007), providing sufficient rainfall for extensive forest growth (Dupont and Weinelt, 1996). A multimodel ensemble result showed an increase in annual mean precipitation during the LIG (Otto-Bliesner et al., 2021), which agrees well with the proxy records over eastern North Africa and the Sahel, but a mismatch occurs over the west and south of North Africa (Scussolini et al., 2019). However, the similarities and differences between the changes in the mean-state climate sensitivity, variability, and mechanism of the NAF monsoon during the LIG and the future warming scenario remain unknown.

Thus, how the NAF monsoon rainfall and variability respond to warming induced by orbital forcing compared to GHG forcing could deepen our understanding of the climate system. Here, we utilize CMIP6 model results to explore the changes in NAF monsoon mean precipitation and its variability during the LIG compared to SSP5-8.5.

2. Data and methods

2.1. Model, observations, and proxy data

We use 12 models from CMIP6/PMIP4 (namely, ACCESS-ESM1-5, CESM2, CNRM-CM6-1, FGOALS-f3-L, FGOALS-g3, GISS-E2-1-G, HadGEM3-GC31-LL, INM-CM4-8, IPSL-CM6A-LR, MIROC-ES2L, NESM3, and NorESM2-LM), which have all performed the SSP5-8.5, PI, and *lig127k* experiments. The last 86 years of each model run from all experiments are used (the period 2015–2100 is used under SSP5-8.5). Since two of the models lack some variables (e.g., vertical velocity and SST), we use at least 10 models (ACCESS-ESM1-5, CESM2, CNRM-CM6-1, FGOALS-f3-L, FGOALS-g3, GISS-E2-1-G, IPSL-CM6A-LR, MIROC-ES2L, NESM3, and NorESM2-LM). The PI experiment is also used in this study. All the variables from CMIP6/PMIP4 are bilinearly interpolated onto a 2.0° × 2.0° horizontal grid to calculate the multimodel ensemble (MME) mean.

For observational datasets, we use monthly precipitation data from the Global Precipitation Climatology centre (GPCC) V2020 with a horizontal resolution of 1.0° × 1.0° (Schneider et al., 2020). The monthly sea level pressure (SLP) data are from the ERA-Interim reanalysis dataset with a 2° horizontal resolution (Dee et al., 2011).

To verify the simulated mean-state SST over the Atlantic during the LIG, we also collect the June–August SST proxies with no drift correction (Fig. S3) (Turney et al., 2020). This LIG SST dataset is from many published SST proxies (e.g., Mg/Ca ratios of calcareous organisms) estimated by several transfer functions (Turney et al., 2020).

2.2. Calendar adjustments

Changes in the eccentricity of Earth's orbit and precession during the LIG can change the month lengths (Bartlein and Shafer, 2019), causing a longer summer and shorter winter in the NH compared to PI. Thus, we use the PaleoCalAdjust program (Bartlein and Shafer, 2019) to conduct calendar adjustments to the modeling results of the *lig127k* experiment prior to analysis.

2.3. Definitions of the NAF monsoon area, variability, and indices

The summer season is defined as June–September (JJAS) in this study. The NAF monsoon is defined by the domain 5°–20°N and 15°W–40°E (Fig. 1(b) and Fig. S1, outlined by green lines). The variability is defined by the standard deviation of the time series (Lu and Fu, 2010). All variables (e.g., SST, precipitation) from SSP5-8.5 and GPCC/ERA-Interim are detrended.

Following Yim et al. (2014), the NAF monsoon circulation index is defined by the 850-hPa zonal winds over (0°–15°N, 60°–10°W), which reflects the strength of the westerly wind across the tropical Atlantic. This index is significantly correlated with the NAF land monsoon precipitation ($R = 0.78$, $p < 0.01$) during the period 1919–2021 (Wang and He, 2021).

In this study, the averaged JJAS SLP over the region (15°–30°N, 55°–5°W) is used to define the westward movement of the Saharan heat low (W-SHL) (Fig. 2(a)), because substantial westward movement of the low-pressure system occurred from the Saharan region to the subtropical North Atlantic Ocean during the LIG period (Fig. S1). The observational data also show that the SHL is significantly linked to the NAF monsoon precipitation (Fig. S4). The westward extension of the SHL is closely related to the West African westerly jet (Pu and Cook, 2010). The SHL-induced cyclonic circulation enhances moist convection and cloud cover in the West African monsoon (Parker et al., 2005). Overall, the SHL can reflect the strength of the NAF monsoon circulation (Biasutti et al., 2009). We use the W-SHL index because the center of the SHL moves to the Atlantic Ocean during the LIG, which is more significant and stronger than that in the SSP5-8.5 scenario (Fig. 2(a, d)). The W-SHL index is used to link the NAF monsoon precipitation variability to the Atlantic SST because of the poor relationship between the NAF monsoon precipitation and the Atlantic SST in the LIG experiment (not shown).

3. Results

3.1. Responses of the NAF monsoon to orbital and GHG forcings

The MME mean shows that the change in the summer surface air temperature (SAT) over the NH is 1.99 °C during the LIG relative to the PI, which is almost two-thirds of the 3.29 °C under SSP5-8.5 (Table 1). Surprisingly, anomalous NAF precipitation increases by 3.44 mm d^{-1} during the LIG and all 12 models agree on the sign (12/12; Table S1), while precipitation only increases by 0.38 mm d^{-1} (10/12) under SSP5-8.5. When scaling the percentage change in precipitation to the NH SAT anomaly, the NAF monsoon precipitation sensitivity is 59.53%/°C under the LIG orbital forcing, which is significantly greater than that (2.8%/°C) under SSP5-8.5 (Table 1).

According to the approximated moisture equation (Jin et al., 2020), a large increase in mean-state rainfall in the LIG is mainly due to a 14.65%/°C increase in specific humidity and 65.39%/°C increase in vertical velocity over the NAF monsoon domain (Table 1). These increases in specific humidity and vertical velocity in the LIG are much greater than those under the SSP5-8.5 scenario, particularly the vertical

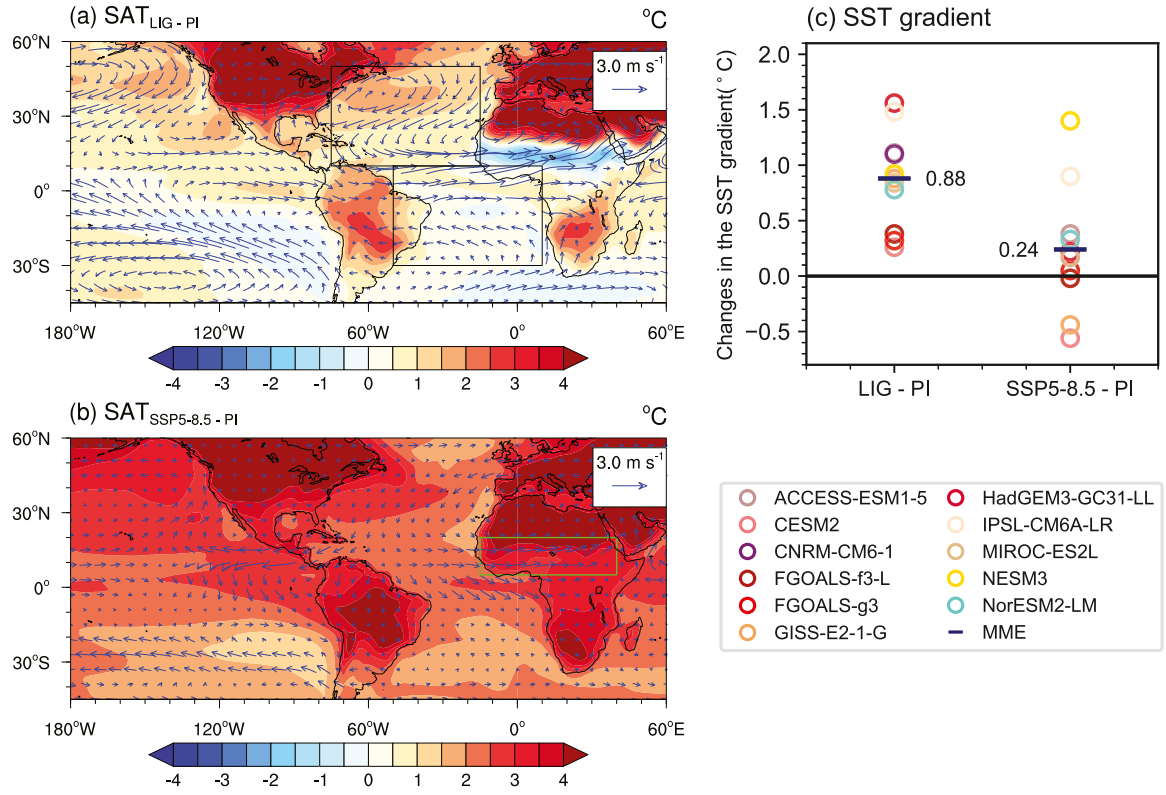

Fig. 1. MME-mean changes in the mean-state JJAS mean SAT (shading; units: °C) and 850-hPa winds (vectors; units: m s^{-1}) in the (a) LIG and (b) SSP5-8.5 scenario, relative to the PI period, respectively. For the SAT anomalies, only significant results with confidence levels exceeding 95% are shown. The two boxes in (a) are used to measure the SST gradient between the North Atlantic (10°–50°N, 75°–15°W) and South Atlantic (30°S–10°N, 50°W–10°E), while the green curves in (b) outline the NAF monsoon region. (c) Changes in the SST gradient (units: °C) in the LIG and SSP5-8.5 scenario relative to the PI period.

Table 1 MME-mean changes in the JJAS-mean SAT over the NH, the specific humidity at 850 hPa, the westerly circulation index, and vertical velocity at 500 hPa over the NAF region, NAF monsoon precipitation, and corresponding variability (σ_P, σ_ω, σ_{ci}) in the LIG and SSP5-8.5 relative to the PI period. An asterisk (*) indicates that at least 70% of models agree on the signal. The change in each model is shown in Tables S2 and S3. The temperature sensitivity is estimated as a 1 °C increase in the JJAS-mean NH SAT. Since the values of the circulation index in the PI period are negative, the changes in the circulation index in the LIG and under SSP5-8.5 are negative.

	NH SAT (°C)	850-hPa specific humidity (%/°C)	Circulation index (%/°C)		500-hPa vertical velocity (%/°C)		Precipitation (%/°C)	
			Average (ci)	Standard deviation (σ_{ci})	Average (ω)	Standard deviation (σ_ω)	Average (P)	Standard deviation (σ_P)
LIG - PI	1.99*	14.65*	−51.74*	8.46*	65.39*	12.01	50.53*	21.55*
SSP5-8.5 - PI	3.29*	8.2*	−5.1*	0.89	1.25	−0.53*	2.8*	4.27*

velocity. Consequently, the response of mean-state NAF monsoon precipitation in the LIG is stronger than that under SSP5-8.5. The equatorial westerlies over the Atlantic Ocean increase substantially by 51.74%/°C during the LIG (Table 1), which brings massive moisture to the NAF region and induces wind convergence over it (Figs. S1(a) and S2(a)). However, the increased westerly is weak (5.1%/°C) and the upward movement is disproportionately small under SSP5-8.5 (Table 1, Fig. S2(c)).

For the monsoon precipitation variability, more summer mean-state rainfall often demonstrates greater variability (Braconnot et al., 2019; Menviel et al., 2021). During the LIG, the NAF monsoon variability increases by 21.55%/°C (11/12), which is much greater than that (4.3%/°C) under SSP5-8.5 (10/12, Table 1 and Fig. S3). Similar to the mean-state precipitation, change in the variability during the LIG primarily results from the enormous increase in the variability of vertical motion (σ_ω, 12.01%/°C, 7/11, Fig. S2(b)), essentially associated with the variability of the westerlies (σ_{ci}, 8.46%/°C, 8/11, Table 1). However, under SSP5-8.5, the variability of vertical motion even decreases by 0.53%/°C (3/11, Table 1, Fig. S2(d)). This is similar to previous findings suggesting that atmospheric moisture dominates the variability of NAF precipitation under the SSP5-8.5 scenario (Zhang et al., 2021). Overall, the mean-state circulation and its variability make decisive contributions to the surges of the mean-state NAF monsoon precipitation and the variability in the LIG, but with little effect under the SSP5-8.5 scenario.

3.2. Oceanic forcing from the Atlantic on the NAF monsoon during the LIG

We first verify the reliability of the simulated SST by comparing climate models with proxy-based reconstructions. Previous studies found that the simulated SST over the North Atlantic is in good agreement with reconstructions (Otto-Bliesner et al., 2021). This study shows that the simulated SST is consistent with reconstructed SST over the extratropical North Atlantic and the South Atlantic, but an overestimated SST occurs over the equatorial Atlantic in climate models (Fig. S3).

To explore the causes of changes in the NAF monsoon mean-state precipitation during the LIG, we check the anomalous SST in the LIG and SSP5-8.5. The result shows that the North Atlantic is warmer than the South Atlantic in the LIG (Fig. 1(a)). This NH-warmer-than-SH pattern over the Atlantic Ocean strengthens the meridional pressure gradient, inducing an anomalous low SLP over the subtropical North Atlantic. This reinforces the northward cross-equatorial flows and pushes

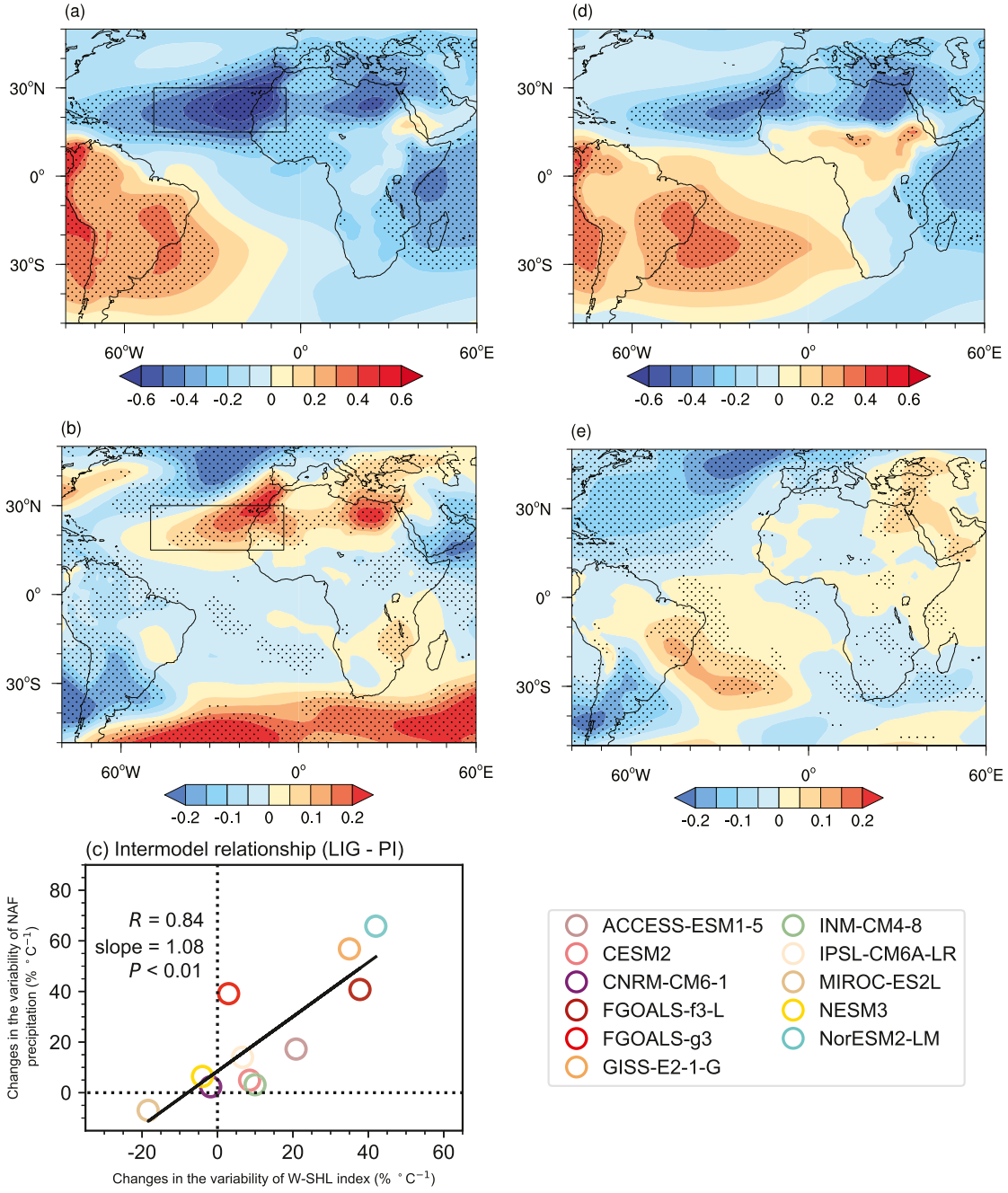

Fig. 2. (a, d) MME-mean correlation maps of the time series of NAF monsoon precipitation with the JJAS-mean SLP in the (a) LIG and (d) SSP5-8.5 scenario. In (a) and (d), significant results with confidence levels exceeding 95% are dotted. (b, e) MME-mean changes in SLP variability during the (b) LIG and (e) SSP5-8.5 scenario relative to the PI period, respectively. In (b) and (e), stippling denotes that at least 70% of models agree on the sign of the MME. The boxes in (a) and (b) define the regions of the W-SHL index in this study. (c) Scatter diagram of the intermodel relationship between the changes in the variability of the W-SHL index and changes in NAF monsoon precipitation variability simulated by 11 CMIP6 models. The solid line denotes linear regression with correlation coefficient *R*, slope, and *P* value.

the ITCZ northward, increasing the NAF mean-state precipitation (Fig. S1(a)). Superimposed on the increased condensational heating due to increased precipitation over the tropical North Atlantic, the deepened SHL expands westward (Fig. S1(a)). This change in the SHL during the LIG is similar to that under the warm AMO phase (Martin and Thorncroft, 2014). The deepening low-pressure change strengthens the westerly across the tropical North Atlantic. The northward cross-equatorial winds are turned to westerlies during the LIG. In contrast, the anomalous meridional SST gradient between the North Atlantic and South Atlantic is weaker under SSP5-8.5. Anomalous equatorial Atlantic warming also occurs, which may decrease the cross-equatorial flows (Fig. 1(b)) and weaken the meridional pressure gradient over the Atlantic Ocean (Fig. S1(b)).

Next, we quantitatively calculate the meridional SST gradient between the North Atlantic and South Atlantic. The anomalous meridional SST gradient increases by 0.88 °C in the LIG, while it only increases by 0.24 °C under SSP5-8.5 (Fig. 1(c)). The increase in the SST gradient in the LIG is approximately 3.67 times that under SSP5-8.5. Then, the circulation index increases by 3.47 m s^{-1} in the LIG, which is approximately 5.65 times that (0.65 m s^{-1}) under SSP5-8.5. This indicates that the anomalous meridional SST gradient plays a critical role in affecting the anomalous westerly winds over the northern tropical Atlantic.

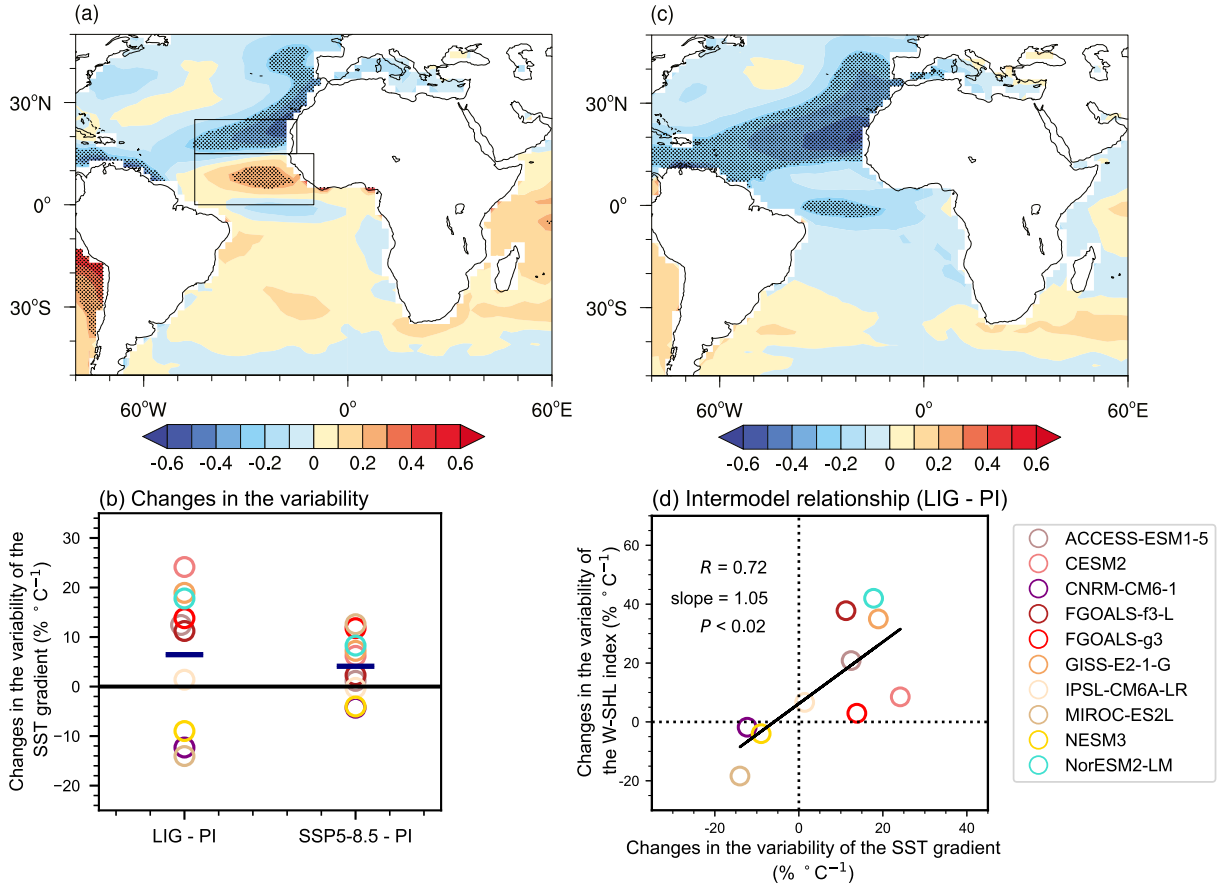

Fig. 3. (a, c) MME-mean correlation maps of the W-SHL index with JJAS SST in the (a) LIG and (c) SSP5-8.5 scenario, respectively. In (a) and (c), the significant results with confidence levels exceeding 95% are dotted. The SST gradient of the correlation coefficient ((15°–25°N, 45°–15°W) minus (0°–15°N, 45°–10°W)) in (a) is outlined. (b) Changes in the variability of the SST gradient in the LIG and SSP5-8.5 relative to the PI period. (d) Intermodel relationship between the changes in the variability of the SST gradient and changes in the variability of the W-SHL index. The solid line denotes linear regression with correlation coefficient *R*, slope, and *P* value.

However, it should be noted that the difference in the increased SST gradient between the LIG and SSP5-8.5 is smaller than the circulation index, which might be influenced by the remote forcing from the Pacific. We notice that the western North Atlantic is warmer than the eastern tropical Pacific during the LIG, which might strengthen the anomalous westerly. In contrast, under SSP5-8.5, the tropical eastern Pacific is warmer than the western North Atlantic, which could induce easterly anomalies and decrease the circulation index (Fig. 1(b)).

To explore the processes of the change in NAF monsoon variability, we check the relationship between the year-to-year time series of the NAF monsoon precipitation and JJAS SLP (Fig. 2(a, b)). The result shows that the NAF monsoon precipitation is significantly correlated with the SLP over the subtropical North Atlantic in the LIG (Fig. 2(a)), but this correlation is much weaker under SSP5-8.5 (Fig. 2(d)). The relationship also exists in the observation but mainly over the Saharan land region (Fig. S4). Furthermore, we use the W-SHL index because the center of the SHL moves westward to the Atlantic Ocean during the LIG. The variability of the W-SHL index increases substantially in the LIG but it decreases under SSP5-8.5 (Fig. 2(b, e)). The intermodel relationship shows that an enhancement of the W-SHL index variability may increase the NAF monsoon precipitation variability in the LIG. Under the SSP5-8.5 scenario, however, the thermodynamic effects (associated with water vapor) dominate the enhancement of NAF monsoon precipitation variability (Zhang et al., 2021).

But why is the variability of the W-SHL index amplified during the LIG? The SST variability could be the main source of climate variability. The El Niño–Southern Oscillation (ENSO) is the strongest signal of interannual variability with global influences, but the ENSO variability decreases significantly in the LIG relative to in the SSP5-8.5 scenario (Brown et al., 2020), which means that the ENSO variability fails to explain the intensified W-SHL index variability. Since the Atlantic oceanic forcing is the primary driver for the interannual NAF precipitation variability (Giannini et al., 2003), we examine the correlations between the time series of the W-SHL index and JJAS SST in the LIG and SSP5-8.5, respectively (Fig. 3). During the LIG, the W-SHL index is significantly correlated with a north–south dipolar SST pattern, with a positive correlation in the tropical North Atlantic and a negative correlation in the subtropical North Atlantic (Fig. 3(a)). The positive correlation means a lower SHL corresponds to a cooler SST west of the NAF land monsoon. On the other hand, the negative correlation implies a lower SHL corresponds to a warmer SST off the coast of the Sahara.

This dipolar SST pattern means an enhanced northward SST gradient. Next, we calculate the variability of the SST gradient over the region (15°–25°N, 45°–15°W) minus (0°–15°N, 45°–10°W) (Fig. 3(a)). The variability of the SST gradient increases by 6.44%/°C in the LIG, but only by 4.1%/°C under SSP5-8.5 (Fig. 3(b)). The increase in the SST gradient variability over the tropical North Atlantic during the LIG is approximately 1.5 times that under SSP5-8.5. We further calculate the variability of the SHL, and results show that it increases by 12.95%/°C during the LIG, which is approximately 10 times larger than that (1.14%/°C) under SSP5-8.5. Additionally, the intermodel relationship indicates that a greater variability of the SST gradient corresponds to a larger variability of the SHL (Fig. 3(d)). Thus, the SST gradient variability is substantially enhanced during the LIG, which may enhance the SHL variability.

The air–sea interaction over the tropical North Atlantic Ocean might enhance during the LIG. One might argue that the greater SST gradient variability causes the SHL variability. However, previous studies suggest that the internal atmospheric variability might also contribute to the precipitation variability (Dong et al., 2018), and thus it is also possible that the SST gradient variability is affected by the Saharan Low variations. An enhanced Sahara Low could increase the westerlies to its south, which could cool the sea surface off the coast of the Sahel, increasing the northward SST gradients. This circular argument implies an atmosphere–ocean interaction that could enhance both the northward SST gradients over the tropical North Atlantic and the Sahara Low. Moreover, the ratio of increase in the W-SHL index variability between the LIG and SSP5-8.5 is a seven-fold increase of the variability in the northward SST gradient. This also implies that there may be a positive feedback of air–sea interaction between the SST gradient variability and the SHL variability. Future work needs to verify whether the atmospheric variability is directly affected by orbital forcing during the LIG.

We therefore provide an alternative explanation for the increased covariability of the northward SST gradients and SHL. It is conceivable that drastically increased NAF mean circulation might enhance the atmosphere–ocean interaction in the tropical North Atlantic off the coast of northern Africa. In the LIG, the climatological SHL shifts dramatically westward to the tropical North Atlantic in association with enhanced westerly monsoon flows and the northward SST gradients in the tropical Atlantic (Fig. 1(a)). This mean-state change could favor atmosphere–ocean interaction to enhance the covariability of the SHL and northward SST gradients, which bears similar spatial patterns to the mean state. This argument is consistent with the observed positive correlation between the mean-state change and the variability change (Pendergrass et al., 2017), and that under future global warming (Zhang et al., 2021).

4. Discussion

A NH-warmer-than-SH pattern over the Atlantic Ocean induces westward expansion and deepening of the SHL and strengthens the westerly along the tropical North Atlantic in the LIG. The westward expansion of the SHL links the SHL to the SST gradients over the northeast tropical Atlantic. Thus, we suggest that the increase in the mean SST gradients between the North and South Atlantic likely reinforces the covariability of the SST gradients and SHL via atmosphere–ocean interaction, leading to an increase in the NAF monsoon variability. Compared to the LIG, this process does not exist under the SSP5-8.5 scenario.

Under the LIG's insolation forcing, the response of the NAF monsoon is much greater than under the SSP5-8.5 scenario and projected by the Clausius–Clapeyron theory (global-mean precipitation increases by 2.2% for every 1 K of warming (Held and Soden, 2006)). The enhancement of the NAF monsoon primarily arises from dynamic effects under orbital forcing. In contrast, the intensification of the NAF monsoon under GHG forcing mainly results from thermodynamic effects (D'Agostino et al., 2019). Compared to thermodynamic effects, dynamic effects have a more powerful influence and amplify thermodynamic effects. Under orbital forcing, the impact of the North Atlantic SST on the NAF monsoon is more robust, and the ocean–atmosphere linkage is significantly strengthened. The interhemispheric SST contrast in the Atlantic during the LIG piques our curiosity about whether the NAF monsoon variability could increase in the warm AMO phase. This deserves further study.

Some uncertainties exist in the models. The *lig127k* simulations adopt the same treatment of vegetation as the PI simulation and neglect the contribution of Saharan vegetation to the intensification of NAF mean rainfall (e.g., Chandan and Peltier, 2020; Sun et al., 2019). Conventional wisdom holds that an increase in NAF monsoon mean rainfall often indicates the enhancement of the variability of NAF monsoon precipitation. Thus, whether the greening of the Sahara would strengthen the NAF monsoon rainfall to reinforce the variability needs to be further studied. Furthermore, some other external forcings or feedback, e.g., soil properties and surface water (Chandan and Peltier, 2020), solar activity (Sun et al., 2022), and dust (Pausata et al., 2016), are not accounted for in the *lig127k* simulation.

5. Conclusions

In this study, the responses of NAF monsoon mean-state rainfall and its variability during the LIG are compared to the SSP5-8.5 scenario based on PMIP4/CMIP6 models. It is found that the NAF monsoon mean-state rainfall and its variability are dramatically stronger in the LIG than under the SSP5-8.5 scenario. In contrast, the NH SAT increases by 1.99 ˚C, which is only about two-thirds of the warming (3.29 ˚C) under SSP5-8.5. In terms of climate sensitivity, the increases in the NAF mean-state rainfall and its variability are approximately 50.53 and 21.55%/˚C during the LIG, which are substantially greater than those (2.8 and 4.27%/˚C) under SSP5-8.5. The significant enhancement of the anomalous westerly and ascending motion and its variability contribute to the intensification of NAF monsoon mean-state precipitation and its variability in the LIG, which mainly arises from the drastic enhancement of the Atlantic north–south SST gradient. This agrees well with the proxy reconstruction. Conversely, the anomalous westerly and ascending motion and their variability in the NAF region are weak under SSP5-8.5, which means that the circulation variability has little effect under this scenario.

Funding

This study was supported by the National Natural Science Foundation of China [grant numbers 42130604, 42105044, 41971108, 42111530182, and 91437218].

Data availability

The file for Dataset S1 is available at https://doi.org/10.6084/m9.figshare.20514645.v5.

Supplementary materials

Supplementary material associated with this article can be found, in the online version, at doi:10.1016/j.aosl.2022.100320.

References

Bartlein, P.J., Shafer, S.L., 2019. Paleo calendar-effect adjustments in time-slice and transient climate-model simulations (PaleoCalAdjust v1.0): impact and strategies for data analysis. Geosci. Model. Dev. 12, 3889–3913. doi:10.5194/gmd-12-3889-2019.

Biasutti, M., Sobel, A.H., Camargo, S.J., 2009. The role of the Sahara low in summertime sahel rainfall variability and change in the CMIP3 models. J. Clim. 22 (21), 5755–5771. doi:10.1175/2009JCLI2969.1.

Braconnot, P., Crétat, J., Marti, O., Balkanski, Y., Caubel, A., Cozic, A., Foujols, M., Sanogo, S., 2019. Impact of multiscale variability on last 6,000 years Indian and West African Monsoon Rain. Geophys. Res. Lett. 46 (23), 14021–14029. doi:10.1029/2019GL084797.

Brown, J.R., Brierley, C.M., An, S.Il, Guarino, M.V., Stevenson, S., Williams, C.J.R., Zhang, Q., et al., 2020. Comparison of past and future simulations of ENSO in CMIP5/PMIP3 and CMIP6/PMIP4 models. Clim. Past 16 (5), 1777–1805. doi:10.5194/CP-16-1777-2020.

Cao, J., Wang, B., Wang, B., Zhao, H., Wang, C., Han, Y., 2020. Sources of the intermodel spread in projected global monsoon hydrological sensitivity. Geophys. Res. Lett. 47, e2020GL089560. doi:10.1029/2020GL089560.

Cao, J., Wang, H., Wang, B., Zhao, H., Wang, C., Zhu, X., 2022. Higher sensitivity of northern hemisphere monsoon to anthropogenic aerosol than greenhouse gases. Geophys. Res. Lett. 49 (20), e2022GL100270. doi:10.1029/2022GL100270.

Chandan, D., Peltier, W.R., 2020. African humid period precipitation sustained by robust vegetation, soil, and lake feedbacks. Geophys. Res. Lett. 47 (21), e2020GL088728. doi:10.1029/2020GL088728.

D'Agostino, R., Bader, J., Bordoni, S., Ferreira, D., Jungclaus, J., 2019. Northern hemisphere monsoon response to mid-holocene orbital forcing and greenhouse gas-induced global warming. Geophys. Res. Lett. 46 (3), 1591–1601. doi:10.1029/2018GL081589.

Dai, A., 2011. Drought under global warming: a review. Wiley Interdiscip. Rev. Clim. Change 2 (1), 45–65. doi:10.1002/WCC.81.

Dee, D.P., Uppala, S.M., Simmons, A.J., Berrisford, P., Poli, P., Kobayashi, S., Andrae, U., 2011. The ERA-Interim reanalysis: configuration and performance of the data assimilation system. Q. J. R. Meteorol. Soc. 137 (656), 553–597. doi:10.1002/QJ.828.

Diakhaté, M., Rodríguez-Fonseca, B., Gómara, I., Mohino, E., Dieng, A.L., Gaye, A.T., 2019. Oceanic forcing on interannual variability of sahel heavy and moderate daily rainfall. J. Hydrometeorol. 20 (3), 397–410. doi:10.1175/JHM-D-18-0035.1.

Dong, L., Leung, L.R., Song, F., Lu, J., 2018. Roles of SST versus internal atmospheric variability in winter extreme precipitation variability along the US West Coast. J. Clim. 31 (19), 8039–8058. doi:10.1175/JCLI-D-18-0062.1.

Dupont, L.M., Weinelt, M., 1996. Vegetation history of the savanna corridor between the Guinean and the Congolian rain forest during the last 150,000 years. Veg. Hist. Archaeobot. 5 (4), 273–292. doi:10.1007/BF00195296.

Folland, C.K., Palmer, T.N., Parker, D.E., 1986. Sahel rainfall and worldwide sea temperatures, 1901–85. Nature 320 (6063), 602–607. doi:10.1038/320602a0.

Giannini, A., Saravanan, R., Chang, P., 2003. Oceanic forcing of sahel rainfall on interannual to interdecadal time scales. Science 302 (5647), 1027–1030. doi:10.1126/SCIENCE.1089357.

Held, I.M., Soden, B.J., 2006. Robust responses of the hydrological cycle to global warming. J. Clim. 19 (21), 5686–5699. doi:10.1175/JCLI3990.1.

Hoerling, M., Hurrell, J., Eischeid, J., Phillips, A., 2006. Detection and attribution of twentieth-century northern and southern African rainfall change. J. Clim. 19 (16), 3989–4008. doi:10.1175/JCLI3842.1.

Hsu, P., Li, T., Murakami, H., Kitoh, A., 2013. Future change of the global monsoon revealed from 19 CMIP5 models. J. Geophys. Res. 118 (3), 1247–1260. doi:10.1002/JGRD.50145.

Jin, C., Wang, B., Liu, J., 2020. Future changes and controlling factors of the eight regional monsoons projected by cmip6 models. J. Clim. 33 (21), 9307–9326. doi:10.1175/JCLI-D-20-0236.1.

Knight, J.R., Folland, C.K., Scaife, A.A., 2006. Climate impacts of the Atlantic multidecadal oscillation. Geophys. Res. Lett. 33, 17706. doi:10.1029/2006GL026242.

Lu, R., Fu, Y., 2010. Intensification of East Asian summer rainfall interannual variability in the twenty-first century simulated by 12 CMIP3 coupled models. J. Clim. 23 (12), 3316–3331. doi:10.1175/2009JCLI3130.1.

Martin, E.R., Thorncroft, C.D., 2014. The impact of the AMO on the West African monsoon annual cycle. Q. J. R. Meteorol. Soc. 140 (678), 31–46. doi:10.1002/qj.2107.

Menviel, L., Govin, A., Avenas, A., Meissner, K.J., Grant, K.M., Tzedakis, P.C., 2021. Drivers of the evolution and amplitude of African Humid Periods. Commun. Earth Environ. 2 (1), 1–11. doi:10.1038/s43247-021-00309-1.

Mohino, E., Janicot, S., Bader, J., 2011. Sahel rainfall and decadal to multi-decadal sea surface temperature variability. Clim. Dyn. 37 (3), 419–440. doi:10.1007/s00382-010-0867-2.

Ni, Y., Hsu, P.C., 2018. Inter-annual variability of global monsoon precipitation in present-day and future warming scenarios based on 33 Coupled Model Intercomparison Project Phase 5 models. Int. J. Climatol. 38 (13), 4875–4890. doi:10.1002/JOC.5704.

O'Neill, B.C., Tebaldi, C., Van Vuuren, D.P., Eyring, V., Friedlingstein, P., Hurtt, G., Knutti, R., et al., 2016. The Scenario Model Intercomparison Project (ScenarioMIP) for CMIP6. Geosci. Model Dev. 9 (9), 3461–3482. doi:10.5194/GMD-9-3461-2016.

Otto-Bliesner, B.L., Braconnot, P., Harrison, S.P., Lunt, D.J., Abe-Ouchi, A., Albani, S., Bartlein, P., et al., 2017. The PMIP4 contribution to CMIP6 - Part 2: two interglacials, scientific objective and experimental design for Holocene and Last Interglacial simulations. Geosci. Model. Dev. 10 (11), 3979–4003. doi:10.5194/GMD-10-3979-2017.

Otto-Bliesner, B.L., Brady, E.C., Zhao, A., Brierley, C.M., Axford, Y., Capron, E., Govin, A., et al., 2021. Large-scale features of Last Interglacial climate: results from evaluating the lig127k simulations for the Coupled Model Intercomparison Project (CMIP6)-Paleoclimate Modeling Intercomparison Project (PMIP4). Clim. Past 17 (1), 63–94. doi:10.5194/cp-17-63-2021.

Parker, D.J., Burton, R.R., Diongue-Niang, A., Ellis, R.J., Felton, M., Taylor, C.M., Thorncroft, C.D., Bessemoulin, P., Tompkins, A.M., et al., 2005. The diurnal cycle of the West African monsoon circulation. Q. J. R. Meteorol. Soc. 131 (611), 2839–2860. doi:10.1256/QJ.04.52.

Pausata, F.S.R., Messori, G., Zhang, Q., 2016. Impacts of dust reduction on the northward expansion of the African monsoon during the Green Sahara period. Earth Planet. Sci. Lett. 434, 298–307. doi:10.1016/J.EPSL.2015.11.049.

Pendergrass, A.G., Knutti, R., Lehner, F., Deser, C., Sanderson, B.M., 2017. Precipitation variability increases in a warmer climate. Sci. Rep. 7 (1), 1–9. doi:10.1038/s41598-017-17966-y.

Pu, B., Cook, K.H., 2010. Dynamics of the West African Westerly Jet. J. Clim. 23 (23), 6263–6276. doi:10.1175/2010JCLI3648.1.

Schneider, U., Becker, A., Finger, P., Rustemeier, E., Ziese, M., 2020. GPCC Full data monthly product version 2020 at 1.0°: monthly land-surface precipitation from rain-gauges built on GTS-based and historical data. doi:10.5676/DWD_GPCC/FD_M_V2020_100.

Scussolini, P., Bakker, P., Guo, C., Stepanek, C., Zhang, Q., Braconnot, P., Cao, J., et al., 2019. Agreement between reconstructed and modeled boreal precipitation of the last interglacial. Sci. Adv. 5 (11), eaax7047. doi:10.1126/sciadv.aax7047.

Sun, W., Liu, J., Wang, B., Chen, D., Wan, L., Wang, J., 2022. Holocene multi-centennial variations of the Asian summer monsoon triggered by solar activity. Geophys. Res. Lett. 49, e2022GL098625. doi:10.1029/2022GL098625.

Sun, W., Wang, B., Zhang, Q., Pausata, F.S.R., Chen, D., Lu, G., Yan, M., Ning, L., Liu, J., 2019. Northern Hemisphere land monsoon precipitation increased by the Green Sahara during middle Holocene. Geophys. Res. Lett. 46 (16), 9870–9879. doi:10.1029/2019GL082116.

Trenberth, K.E., Stepaniak, D.P., Caron, J.M., 2000. The global monsoon as seen through the divergent atmospheric circulation. J. Clim. 13 (22), 3969–3993. doi:10.1175/1520-0442(2000)013<3969:TGMAST>2.0.CO;2.

Turney, C.S.M., Jones, R.T., McKay, N.P., Van Sebille, E., Thomas, Z.A., Hillenbrand, C.D., Fogwill, C.J., 2020. A global mean sea surface temperature dataset for the Last Interglacial (129-116ka) and contribution of thermal expansion to sea level change. Earth Syst. Sci. Data 12 (4), 3341–3356. doi:10.5194/ESSD-12-3341-2020.

Wang, B., He, Q., 2021. Global monsoon summary. In: State of the climate in 2021. Bull. Am. Meteorol. Sci. 103 (8), S210–S213. doi:10.1175/BAMS-D-22-0069.1.

Wang, B., Biasutti, M., Byrne, M.P., Castro, C., Chang, C.P., Cook, K., Fu, R., et al., 2021. Monsoons climate change assessment. Bull. Am. Meteorol. Soc. 102 (1), E1–E19. doi:10.1175/BAMS-D-19-0335.1.

Weldeab, S., Lea, D.W., Schneider, R.R., Andersen, N., 2007. 155,000 Years of West African monsoon and ocean thermal evolution. Science 316 (5829), 1303–1307. doi:10.1126/science.1140461.

Yim, S. Y., Wang, B., Liu, J., Wu, Z, 2014. A comparison of regional monsoon variability using monsoon indices, Clim. Dyn. 43(5), 1423-1437. doi:10.1007/s00382-013-1956-9.

Zhang, W., Furtado, K., Wu, P., Zhou, T., Chadwick, R., Marzin, C., Rostron, J., Sexton, D., 2021. Increasing precipitation variability on daily-to-multiyear time scales in a warmer world. Sci. Adv. 7 (31), eabf8021. doi:10.1126/SCIADV.ABF8021.